

Continuous variable entanglement in a cold-atoms mirrorless optical parametric oscillator

G. C. Borba,^{1,2} R. S. N. Moreira,^{1,3} L. S. Cruz,⁴ M. Martinelli,² D. Felinto,¹ and J. W. R. Tabosa¹

¹*Departamento de Física, Universidade Federal de Pernambuco, 50670-901 Recife, PE, Brazil*

²*Instituto de Física da Universidade de São Paulo, P.O. Box 66318, 05315-970 São Paulo, Brazil*

³*Centro de Ciências, Tecnologia e Saúde, Universidade Estadual da Paraíba, 58233-000 Araruna, PB, Brazil*

⁴*Centro de Ciências Naturais e Humanas, Universidade Federal do ABC, Santo André, São Paulo, 09210-170, Brazil*

(Dated: December 30, 2024)

In this work, we explore both the internal and external atomic degrees of freedom to observe entanglement between the modes produced by a mirrorless optical parametric oscillator (MOPO) operating below the oscillation threshold in a sample of free space cold cesium atoms. The platform allows the generation of multipartite entanglement among many optical modes that could potentially be used in quantum network technologies.

A nonlinear optical medium can efficiently generate forward and backward waves through parametric processes, conserving energy and momentum between input and output fields. The first proposal to use this principle to achieve mirrorless optical oscillation, almost sixty years ago, considered a three-wave-mixing process in a medium with second-order $\chi^{(2)}$ nonlinearity [1]. The implementation of this original idea succeeded only in 2007 [2], using quasi phase-matching in a nonlinear photonic structure to satisfy its stringent phase-matching requirements. In 1977, a decade after the original proposal, it was shown that the four-wave mixing process, employing a third-order $\chi^{(3)}$ nonlinearity, could also result in mirrorless optical oscillation [3]. Since the phase-matching requirements were much easier to achieve in this case, in the following year, the first experimental observation of mirrorless oscillation in four-wave mixing was already reported [4]. Since then, in the last four decades, many groups have experimentally observed the formation of a mirrorless optical parametric oscillator (MOPO) in four-wave mixing in different physical systems [5–16]. The MOPO based on both kinds of nonlinearities may work as robust and self-aligned coherent light sources analogous to distributed feedback lasers [2, 17, 18]. In addition, the $\chi^{(2)}$ MOPO provides tunable coherent light sources covering wavelengths in the terahertz [19] and near-infrared regions [20], while the less-stringent phase-matching condition of the $\chi^{(3)}$ MOPO is well suited for the self-established formation of cascaded parametric oscillations in multiple directions [5, 8, 9, 12, 16].

On the other hand, optical parametric oscillators (OPOs) have been established as a standard platform to generate non-classical states in continuous variables. From the squeezed vacuum in sub-threshold operation [21] to the twin beam generation [22], and the entanglement generation below [23] and above [24] threshold, these systems soon found applications in construction of networks of entangled states, directly coupling distinct modes, discriminated either in time [25], frequency [26] or wavelength [27]. Use of third-order nonlinearity, on

the other hand, led to the possibility of integrating those devices, resulting in on-chip manipulation of quantum states that led to demonstrations of quantum advantage [28].

We show that a mirrorless OPO based on the four-wave mixing process in an atomic cloud [16] can produce entangled fields from the parametric amplification of vacuum input. Moreover, since the process involves the coupling of multiple input fields, the possibility of multimode entanglement is discussed based on the purity of the measured system, indicating a more extensive network of entangled states.

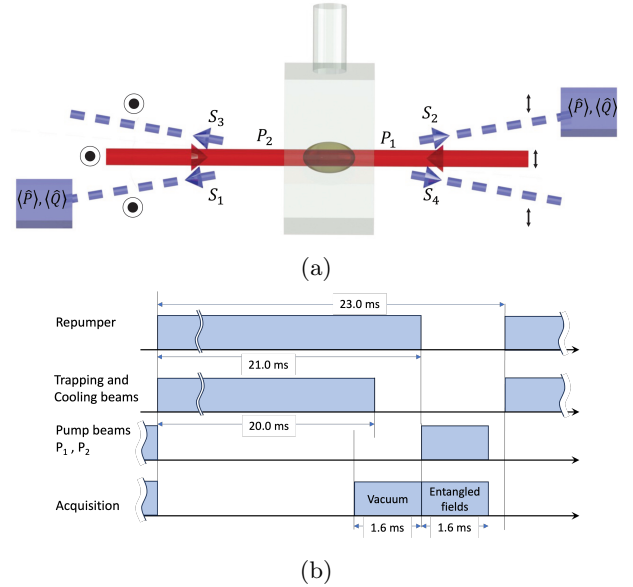


FIG. 1: (a) Simplified experimental setup. The counter-propagating pumping beams (P_1 and P_2) with linear orthogonal polarizations interact with the atoms and generate the four modes specified by $S_1, S_2, S_3,$ and S_4 . Modes S_1, S_2 are sent to two independent heterodyne detection systems. (b) Time sequence of the involved fields and detection process.

The MOPO involves two counter-propagating pump beams (P_1 and P_2) with the same frequency ω and orthogonal linear polarizations, as depicted in Fig. 1, over a cloud of cold Cesium atoms. For such beam geometry interacting nearly in resonance with a degenerate two-level system, multiple FWM processes can take place associated with Zeeman coherence as well as coherences between momentum states via recoil-induced resonance (RIR) [30]. In these conditions, it has been demonstrated that a probe field can be amplified by a factor exceeding 2000 due a feedback loop [16].

The dynamic of the pairwise photon creation involving the four modes can be understood with a combination of parametric amplifiers, and the Hamiltonian of this process can be written as

$$\hat{H}_I = i\hbar [\chi_{12}\hat{a}_1\hat{a}_2 + \chi_{34}\hat{a}_3\hat{a}_4 + \chi_{24}\hat{a}_2\hat{a}_4 + \chi_{13}\hat{a}_1\hat{a}_3 - \text{H.c.}], \quad (1)$$

using the field operators for modes 1-4. A useful approach considering balanced couplings in the 4WM process, such that $\chi_{ij} = \chi$, allows for a simple substitution in the operators, as $\hat{a}_a = (\hat{a}_1 + \hat{a}_4)/\sqrt{2}$, $\hat{a}_b = (\hat{a}_2 + \hat{a}_3)/\sqrt{2}$, resulting in

$$\hat{H}_I = i\hbar\chi [\hat{a}_a\hat{a}_b - \text{H.c.}]. \quad (2)$$

In this case, one can observe that we have the generation of photon pairs on a mode given by a combination of modes 1 and 4 and another in a combination of modes 2 and 3, corresponding to a Bloch-Messiah decomposition involving two-mode squeezing states [30]. As first approach to the system, we started by the evaluation of entanglement involving just a pair of modes, as shown in Fig.1.

The experiment is performed in a cold cloud of cesium atoms obtained from a magneto-optical trap (MOT) using the Zeeman structure of the hyperfine levels $6S_{1/2}(F = 4)$ and $6P_{3/2}(F' = 5)$. The trap (cooling beam, repump beam, and magnetic quadrupole field) are kept on for 20 ms, then followed by a 1 ms cycle of repump (Fig. 1), resulting in a cold sample of Cs atoms in the $6S_{1/2}(F = 4)$ ground state, with about 2 mm diameter, optical density of 5, and temperature in hundreds of μK range. Three pairs of Helmholtz coils are employed to compensate for residual magnetic fields, whose current values are adjusted by optimization of microwave spectroscopy [32] in the cesium clock transition $6S_{1/2}(F = 3) \rightarrow 6S_{1/2}(F = 4)$.

Differently from the configuration in [16], we use a probe beam only for alignment purposes [30] and only measure the spontaneous process. The pump beams P_1 and P_2 have approximately the same waist diameter of 1.6 mm and are switched on during the period of 1.6 ms after turning off all MOT beams and trapping magnetic field. Pump beams are provided by a

Ti:sapphire laser locked to a saturated absorption signal and their frequencies are shifted by an acoustic-optic modulator (AOM) detuned around $\Delta = 25\text{MHz} (\approx 5\Gamma)$ below the resonance frequency of the cesium closed transition $6S_{1/2}, F = 4 \rightarrow 6P_{3/2}, F' = 5$

The measurement of the field uses a heterodyne detection based on the interference of the amplified vacuum with an optical field, shifted by 5 MHz from the pump frequency, used as an optical local oscillator in a balanced detection. Subtraction of the photodiode's currents is further demodulated by a pair of in-quadrature electronic references at the shift frequency, thus providing a combined measurement of both quadratures of the signal of interest, plus one unit of vacuum [30]. The resulting measurement of the quadrature for each field is recorded by an analog-to-digital converter and the statistics is further performed, in order to recover the covariance matrix of the signal.

Differently from the majority of the CV systems, which have a continuous generation of the fields, a measurement involving the cold cloud is performed when the trapping fields are turned off and the cloud is left for free expansion. Given the narrow bandwidth of the RIR resonances (on the order of 20 kHz [16]), there is a lower limit for the repetition rate of the measurements. In our case, an acquisition time shorter than 25 μs implies in correlation of sequential measurements and data redundancy. On the other hand, the upper limit for the acquisition cycle is given by free-expansion of the cloud. A reasonable time of 1.6 ms results in a total of 64 acquired values of the quadratures for each run of the MOT. Precise calibration of the standard quantum level, used as our normalization factor in the present results, is assured by running a previous cycle of acquisition before turning on the pump fields (Fig. 1). The resulting input on the detection has only vacuum fluctuations, since all the involved fields (pump, trap and repump) are turned off, as was experimentally verified by evaluation at distinct powers of the local oscillator. By repeating the cycles of trapping, cooling and acquisition, enough data is acquired to evaluate the variances of the quadratures for distinct values of the pump beams.

Evaluation of the variances of the quadratures is directly performed from the acquired data, normalized to the observed variance for the vacuum input. The result, presented in Fig. 2, is compared with the simple model of parametric amplification derived from Eq. 1. It is clear that, while a parametric amplifier is expected to give a gain over the vacuum input that evolves with the pump as a hyperbolic cosine, the mirrorless parametric oscillator provides a stronger amplification, noticeably deviating from the expected behavior at small pump intensities. This dramatic behavior is reminiscent of the huge gain observed in this system [16], that can reach self-oscillatory regime for modest driving of the pumps. A detailed model for the mirrorless OPO, including the

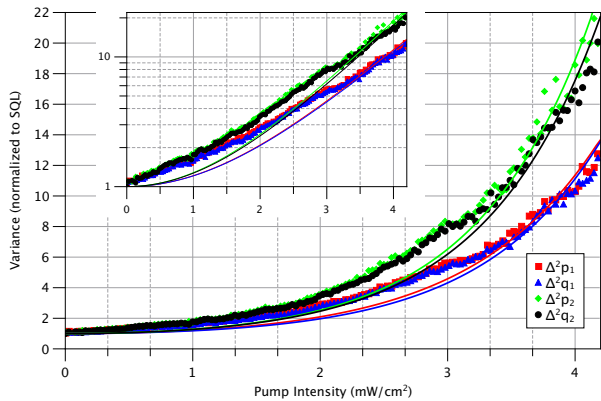


FIG. 2: Variances of field quadratures as function of the pump intensity (of a single beam). The fits follow the model of the parametric amplifier. Inset: the same curve on log vertical scale.

details of the atomic dynamic, is left for future studies. The power unbalance between the generated modes can be understood as a consequence of eventual imbalance in the couplings χ_{ij} [30]. It is experimentally observed, upon the injection of a seed, that the power of the generated fields are sensitive to alignment of the pump beams, directly affecting this coupling. This behavior can be analyzed, following the description of the process given by Eq. 1, using a Bloch-Messiah decomposition [30]. The same model can be used for the evaluation of entanglement and purity of the generated state, parametrizing the results by the average gain of both channels (S_1 and S_2), calculated from the evaluated variances in Fig. 2.

The entanglement properties of Gaussian states can be completely characterized by their second-order moments, which can be conveniently organized as a covariance matrix $\mathbb{V} = \left\langle \hat{\xi}\hat{\xi}^T + \left(\hat{\xi}\hat{\xi}^T \right)^T \right\rangle / 2$, where

$$\hat{\xi} = (\hat{p}_1, \hat{q}_1, \hat{p}_2, \hat{q}_2)^T. \quad (3)$$

The covariance matrix can be divided into three 2×2 submatrices, from which two (\mathbb{A}_j) represent the reduced covariance matrices of the individual subsystems and one (\mathbb{C}) expresses the correlations between the subsystems

$$\mathbb{V} = \begin{pmatrix} \mathbb{A}_1 & \mathbb{C} \\ \mathbb{C}^T & \mathbb{A}_2 \end{pmatrix}. \quad (4)$$

Here, the expected covariance matrix from Eq.1, reduced for modes 1 and 2 only, will be given by

$$\mathbb{V} = \left[\begin{array}{c|c} a_1 & c \\ \hline a_1 & -c \\ \hline c & a_2 \\ \hline -c & a_2 \end{array} \right]. \quad (5)$$

Entanglement can be probed by the positive partial transposition (PPT) criterion, which is commonly stated

in terms of the symplectic eigenvalues of the partially transposed (PT) covariance matrix [33]. In the present case, however, the direct evaluation of each term of the covariance matrix given by Eq. 4 suffers from the precise reproducibility conditions of the MOT on each cycle. Averaging over distinct MOT runs does not affect the main diagonal terms of the covariance matrix, but the covariances in the correlation matrix \mathbb{C} vanish due to random phase shifts resulting from small cloud displacements on each run of the trapping cycle. On the other hand, the determinants of the covariance matrix are invariant under rotations [33] associated to these phase shifts. Therefore, for each MOT cycle, the correlations are evaluated, the determinant of \mathbb{C} is calculated, and an average over multiple acquisitions returns the expected value of $\text{Det}[\mathbb{C}]$. As we will see, the determinants are sufficient for the observation of entanglement and evaluation of the purity.

Using the Robertson-Schrödinger uncertainty relation

$$\mathbb{V} + i\Omega \geq 0 \quad \text{with} \quad \Omega = \bigoplus_{i=1}^2 \begin{bmatrix} 0 & 1 \\ -1 & 0 \end{bmatrix}, \quad (6)$$

the condition for physicality of the covariance matrix can be recast in terms of the determinants of the submatrices as [33, 34]

$$W = 1 + \text{Det}[\mathbb{V}] - 2\text{Det}[\mathbb{C}] - \text{Det}[\mathbb{A}_1] - \text{Det}[\mathbb{A}_2] \geq 0. \quad (7)$$

The partial transposition modifies the sign of $\text{Det}[\mathbb{C}]$, resulting in the following sufficient and necessary condition for entanglement in bipartite Gaussian states:

$$W_{\text{PPT}} = 1 + \text{Det}[\mathbb{V}] + 2\text{Det}[\mathbb{C}] - \text{Det}[\mathbb{A}_1] - \text{Det}[\mathbb{A}_2] < 0. \quad (8)$$

Another relevant quantity is the purity of a quantum state, defined as $\mu = \text{Tr}[\rho^2] \leq 1$. It can be evaluated from the determinant of the covariance matrix \mathbb{M} for Gaussian states as $\mu = 1/\sqrt{\text{Det}[\mathbb{V}]}$ [37]. In the present case, given the symmetry of the resulting covariance (Eq. 5), the determinant of the matrix \mathbb{V} can be evaluated as

$$\text{Det}[\mathbb{V}] = \left(\sqrt{\text{Det}[\mathbb{A}_1]\text{Det}[\mathbb{A}_2]} - |\text{Det}[\mathbb{C}]| \right)^2. \quad (9)$$

Thus, evaluation of the determinants $\text{Det}[\mathbb{A}_1]$, $\text{Det}[\mathbb{A}_2]$, and $\text{Det}[\mathbb{C}]$ for distinct pump intensities, and therefore for distinct gains of the parametric amplification, is useful for the test of entanglement and purity of the generated states.

Figure 3 presents the evaluated determinants, as a function of the average gain obtained from the results in Fig. 2. Results are presented for pump intensities up to 1.6 mW/cm². Starting from unity gain, as expected for a vacuum state, they grow with the pump power. The imbalance of determinants for \mathbb{A}_1 and \mathbb{A}_2 is modeled by distinct couplings in the Bloch-Messiah decomposition [30], being the only fitting parameter for the model.

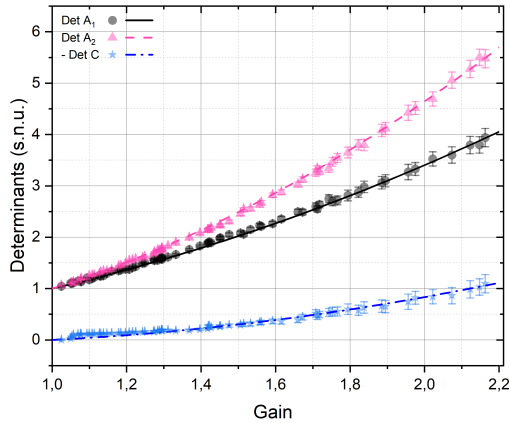


FIG. 3: Measured values for the determinants of the covariance matrices of fields 1 ($\text{Det}[A_1]$) and 2 ($\text{Det}[A_2]$), and cross-correlations ($-\text{Det}[C]$), and the fits according to the model.

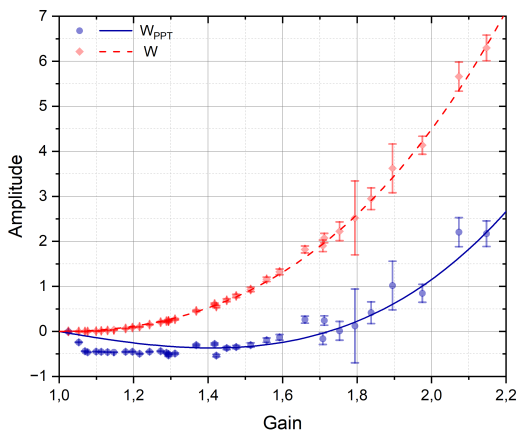


FIG. 4: Physicality test of the measured covariance matrix (W) entanglement witness (W_{PPT}), evaluated from the data in Fig. 3

Notice that $\text{Det}[C] < 0$ over the entire range, fulfilling a necessary condition for entanglement [33]. The model of the curve for $\text{Det}[C]$ considers a mode mismatch of 0.65 between amplified vacuum modes at the heterodyne measurement, as described in [30].

These results allow the evaluation of the entanglement witness W_{PPT} , along with the physicality test of the covariance matrix W , as presented in Fig. 4. We can notice that, for a gain smaller than 1.7, entanglement of the pair of modes is observed. The loss of entanglement for higher gains comes from the imperfect matching of the modes on the detection.

A relevant aspect of the system is shown in the evalu-

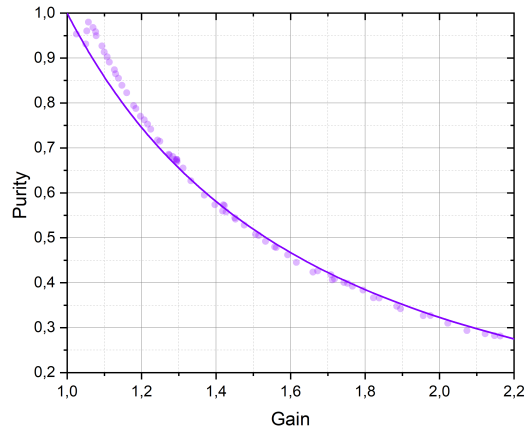


FIG. 5: Purity, evaluated from the data in Fig. 3

ation of the purity of the state. As we can see in Fig. 5, as the gain increases, the purity decreases monotonically. This is a direct consequence of the fact that our detection system is looking at just a pair of the modes in this parametric amplification involving, at least, four channels. Since we are tracing over the remaining modes (3 and 4), this loss of information is leading to a degradation of the purity. Since parametric amplification is a unitary process, this loss of purity of the partial system can be associated with an increase in the correlations with the traced part. It is our expectation that, under the full measurement of the involved modes, a rich structure of entanglement can thus be recovered, and the observed results, presented here for modes 1 and 2, will be present in pairwise analyses involving pairs of modes (3,4), (1,3), and (2,4) as well.

CONCLUSIONS

The amplification of vacuum modes by a mirrorless optical parametric oscillator led to the generation of entangled pair of modes with narrow linewidth using a cold cloud of Cs atoms as a gain medium.

The analysis of the purity in this system is consistent with the fact that we are detecting, for the moment, just two of the four generated modes. Therefore, a richer structure of entanglement is expected involving four modes of the field.

Moreover, as demonstrated in the previous work of the group, the driven atomic cloud has memory [36]. Therefore, it should be possible to have this system as a key component in quantum networks, using the possibility to generate large-scale spatially separated entanglement using both spatial and time multiplexing for applications in quantum information.

ACKNOWLEDGEMENTS

This study was financed, in part, by the São Paulo Research Foundation (FAPESP), Brasil. Process Number #2018/20159-8, #2021/06535-0, #2022/09436-5; Office of Naval Research (N62909-23-1-2014). Conselho Nacional de Desenvolvimento Científico e Tecnológico (INCT-IQ 465469/2014-0); Coordenação de Aperfeiçoamento de Pessoal de Nível Superior (PROEX 23038.003069/2022-87); Fundação de Amparo à Ciência e Tecnologia do Estado de Pernambuco (APQ-0616-1.05/18);

-
- [1] S. E. Harris, Proposed backward wave oscillation in the infrared, *App. Phys. Lett.* **9**, 114-116 (1966).
- [2] C. Canalias and V. Pasiskevicius, Mirrorless optical parametric oscillator, *Nat. Photonics* **1**, 459-462 (2007).
- [3] A. Yariv and D. M. Pepper, Amplified reflection, phase conjugation, and oscillation in degenerate four-wave mixing, *Opt. Lett.* **1**, 16-18 (1977).
- [4] D. M. Pepper, D. Fekete, and A. Yariv, Observation of amplified phase-conjugate reflection and optical parametric oscillation by degenerate four-wave mixing in a transparent medium, *Appl. Phys. Lett.* **33**, 41-44 (1978).
- [5] N. Tan-No, T. Hoshimiya, and H. Inaba, Dispersion-Free Amplification and Oscillation in Phase-Conjugate Four-Wave Mixing in an Atomic Vapor Doublet, *IEEE J. Quantum Electron.* **QE-6**, 147-153 (1980).
- [6] S. G. Odulov, S. S. Slyusarenko, and M. S. Soskin, Laser with dynamic gratings of free carriers in a semiconductor, *Sov. J. Quantum Electron.* **14**, 589-590 (1984).
- [7] J. R. R. Leite, P. Simoneau, D. Bloch, S. Le Boiteux, and M. Ducloy, Continuous-Wave Phase-Conjugate Self-Oscillation Induced by Na-Vapour Degenerate Four-Wave Mixing With Gain, *Europhys. Lett.* **2**, 747-753 (1986).
- [8] S. Odoulov, R. Jungen, and T. Tschudi, Mirrorless Coherent Oscillation Due to Vectorial Four-Wave Mixing in LiNbO_3 , *Appl. Phys. B* **56**, 57-61 (1993).
- [9] J. Neumann, G. Jäkel, and E. Krätzig, Holographic scattering lines and mirrorless oscillation in BaTiO_3 , *Opt. Lett.* **20**, 1530-1532 (1995).
- [10] A. S. Zibrov, M. D. Lukin, and M. O. Scully, Nondegenerate Parametric Self-Oscillation via Multiwave Mixing in Coherent Atomic Media, *Phys. Rev. Lett.* **83**, 4049-4052 (1999).
- [11] Y. Uesu, K. Yasukawa, N. Saito, S. Odoulov, K. Shcherbin, A. I. Ryskin, and A. S. Shcheulin, Backward-wave four-wave mixing and coherent oscillation in $\text{CdF}_2\text{:Ga,Y}$, *Appl. Phys. B* **78**, 601-605 (2004).
- [12] K. Harada, M. Ogata, and M. Mitsunaga, Four-wave parametric oscillation in sodium vapor by electromagnetically induced diffraction, *Opt. Lett.* **32**, 1111-1113 (2007).
- [13] J. A. Greenberg and D. J. Gauthier, Steady-state, cavityless, multimode superradiance in a cold vapor, *Phys. Rev. A* **86**, 013823 (2012).
- [14] K. Zhang, J. Guo, C.-H. Yuan, L. Q. Chen, C. Bian, B. Chen, Z. Y. Ou, and W. Zhang, Mirrorless parametric oscillation in an atomic Raman process, *Phys. Rev. A* **89**, 063826 (2014).
- [15] Y. Mei, X. Guo, L. Zhao, and S. Du, Mirrorless Optical Parametric Oscillation with Tunable Threshold in Cold Atoms, *Phys. Rev. Lett.* **119**, 150406 (2017).
- [16] J. P. Lopez, A. M. G. de Melo, D. Felinto, and J. W. R. Tabosa, Observation of giant gain and coupled parametric oscillations between four optical channels in cascaded four-wave mixing, *Phys. Rev. A* **100**, 023839 (2019).
- [17] S. G. Odulov, S. S. Slyusarenko, M. S. Soskin, and A. I. Khizhnyak, Mirror-free four-wave parametric oscillation in CdTe crystals, *Sov. J. Quantum Electron.* **18**, 977-980 (1988).
- [18] J. B. Khurgin, Mirrorless magic, *Nature Photon* **1**, 446-447 (2007).
- [19] K. Nawata, Y. Tokizane, Y. Takida, and H. Minamide, Tunable Backward Terahertz-wave Parametric Oscillation, *Sci. Rep.* **9**, 726 (2019).
- [20] K. M. Molster, M. Guionie, P. Mutter, J.-B. Dherbecourt, J.-M. Melkonian, X. Delen, A. Zukauskas, C. Canalias, F. Laurell, P. Georges, M. Raybaut, A. Godard, and V. Pasiskevicius, Pump Tunable Mirrorless OPO: an Innovative Concept for Future Space IPDA Emitters. ICSSO (International Conference on Space Optics) 2022, Oct 2022, Dubrovnik, Croatia..
- [21] L. A. Wu, H. J. Kimble, J. L. Hall, and H. F. Wu, "Generation of squeezed states by parametric down conversion," *Phys. Rev. Lett.* **57**, 2520-2523, (1986).
- [22] A. Heidmann, R. J. Horowicz, S. Reynaud, E. Giacobino, C. Fabre, and G. Camy, "Observation of quantum noise reduction on twin laser beams," *Phys. Rev. Lett.* **59**, 255-257 (1987).
- [23] Z. Y. Ou, S. F. Pereira, H. J. Kimble, and K. C. Peng, "Realization of the Einstein-Podolsky-Rosen paradox for continuous variables," *Phys. Rev. Lett.* **68**, 3663-3666, (1992).
- [24] A. S. Villar, L. S. Cruz, K. N. Cassemiro, M. Martinelli, and P. Nussenzweig, "Generation of Bright Two-Color Continuous Variable Entanglement" *Phys. Rev. Lett.* **95**, 243603 (2005).
- [25] S. Yokoyama, R. Ukai, S. C. Armstrong, C. Sornphiphatphong, T. Kaji, S. Suzuki, J. Yoshikawa, H. Yonezawa, N. C. Menicucci, and A. Furusawa, "Ultra-large-scale continuous-variable cluster states multiplexed in the time domain," *Nature Photonics* **7**, 982-986 (2013).
- [26] M. Chen, N. C. Menicucci, and O. Pfister, "Experimental Realization of Multipartite Entanglement of 60 Modes of a Quantum Optical Frequency Comb," *Phys. Rev. Lett.* **112**, 120505 (2014).
- [27] Y. Cai, J. Roslund, G. Ferrini, F. Arzani, X. Xu, C. Fabre, and N. Treps, "Multimode entanglement in reconfigurable graph states using optical frequency combs," *Nature Communications* **8**, 15645 (2017).
- [28] Madsen, L.S., Laudenbach, F., Askarani, M.F. et al. Quantum computational advantage with a programmable photonic processor. *Nature* **606**, 75-81 (2022)
- [29] A. Schilke, C. Zimmermann, P. W. Courteille, and W. Guerin, *Optical parametric oscillation with distributed feedback in cold atoms*, *Nature Photonics* **6**, 101 (2011).
- [30] See Supplemental Material at URL-will-be-inserted-by-publisher.

- [31] A. S. Coelho, F. A. S. Barbosa, K. N. Cassemiro, A. S. Villar, M. Martinelli, and P. Nussenzveig, *Three-color entanglement*, *Science* **326**, 823 (2009).
- [32] A. J. F. de Almeida, M.-A. Maynard, C. Banerjee, D. Felinto, F. Goldfarb, and J. W. R. Tabosa, *Nonvolatile optical memory via recoil-induced resonance in a pure two-level system*, *Phys. Rev. A* **94**, 063834 (2016).
- [33] R. Simon, *Peres-horodecki separability criterion for continuous variable systems*, *Phys. Rev. Lett.* **84**, 2726 (2000).
- [34] F. A. S. Barbosa, A. J. de Faria, A. S. Coelho, K. N. Cassemiro, A. S. Villar, P. Nussenzveig, and M. Martinelli, *Disentanglement in bipartite continuous-variable systems*, *Phys. Rev. A* **84**, 052330 (2011).
- [35] M. G. A. Paris, F. Illuminati, A. Serafini, and S. De Siena, *Purity of gaussian states: Measurement schemes and time evolution in noisy channels*, *Phys. Rev. A* **68**, 012314 (2003).
- [36] J. P. Lopez, A. M. G. de Melo, and J. W. R. Tabosa, *Self-amplifying memory based on multiple cascading four-wave mixing via recoil-induced resonance*, *Optics Letters* **45**, 3490 (2020).
- [37] G. Adesso, A. Serafini, and F. Illuminati, *Entanglement, purity, and information entropies in continuous variable systems*, *Open Syst. Inf. Dyn.* **12**, 189–205 (2005).

Supplemental Material: Continuous variable entanglement in a cold-atoms mirrorless optical parametric oscillator

I. MODELING OF THE PARAMETRIC PROCESS

A first approach to the Four-Wave mixing (FWM) process using Recoil-Induced Resonance (RIR) can consider four distinct parametric amplifiers, as described by the interaction Hamiltonian

$$\hat{H}_I = i\hbar [\chi_{12}\hat{a}_1\hat{a}_2 + \chi_{34}\hat{a}_3\hat{a}_4 + \chi_{24}\hat{a}_2\hat{a}_4 + \chi_{13}\hat{a}_1\hat{a}_3 - \text{H.c.}]. \quad (1)$$

We can calculate the evolution of the operators as

$$\frac{d}{dt}\vec{A} = \frac{i}{\hbar} [\hat{H}_I, \vec{A}] = \mathbb{M}\vec{A} \quad (2)$$

with $\vec{A} = (\hat{a}_1, \hat{a}_2, \hat{a}_3, \hat{a}_4, \hat{a}_1^\dagger, \hat{a}_2^\dagger, \hat{a}_3^\dagger, \hat{a}_4^\dagger)$ and \mathbb{M} as

$$\mathbb{M} = \begin{bmatrix} 0 & \mathbb{X} \\ \mathbb{X} & 0 \end{bmatrix}, \quad \text{with} \quad \mathbb{X} = \begin{bmatrix} 0 & \chi_{12} & \chi_{13} & 0 \\ \chi_{12} & 0 & 0 & \chi_{24} \\ \chi_{13} & 0 & 0 & \chi_{34} \\ 0 & \chi_{24} & \chi_{34} & 0 \end{bmatrix}. \quad (3)$$

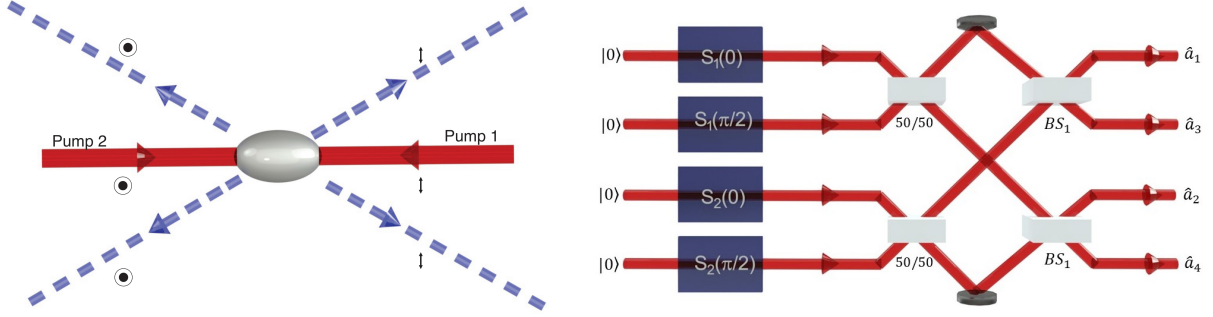


FIG. 1: Left: Four-wave mixing process, with the labeling of the generated fields and their polarization. Right: The corresponding Bloch-Messiah decomposition.

The covariance matrix involving the quadratures of the fields, our final subject of analysis in this paper, can be obtained from the evolution of the operators in Equation 2. The result will depend strongly with the values of the four coupling terms χ_{ij} , that on their turn should be dependent on the power of the pump fields, their overlap with the amplified modes, atomic density and temperature, not to mention residual magnetic fields. The delicate control of these parameters can be observed by injection of a seed in one of the channels [2]. The measured power of the four generated modes and their relative values will present strong dependency on the alignment of the pump beams, even if extreme care is taken on the balance of their power and matching of their waist position and size on the center of the atomic cloud.

A good insight on the problem can be brought when we consider that $\chi_{ij} = \chi$, thus a balanced coupling on the four processes. In this case, diagonalization leads directly to a pair of eigenmodes, $\hat{a}_+ = [(\hat{a}_1 + \hat{a}_4) + (\hat{a}_2 + \hat{a}_3)]/2$ and $\hat{a}_- = [(\hat{a}_1 + \hat{a}_4) - (\hat{a}_2 + \hat{a}_3)]/2$, associated to compression by a term associated to $\exp(\pm\chi\tau)$, where τ is the time of flight inside the interaction region, and two other independent terms, $(\hat{a}_1 - \hat{a}_4)/\sqrt{2}$ and $(\hat{a}_2 - \hat{a}_3)/\sqrt{2}$, associated to null eigenvalues.

Extension to the general case can be performed by a Bloch-Messiah decomposition [3], as shown in Figure 1. From the diagonalization of matrix \mathbb{X} , a set of eigenvalues $(r_1, -r_1, r_2, -r_2)$ with only two independent terms is obtained. This is consistent with a first stage of squeezing operators $S_i(\theta)$, where the quadratures of the compressions $(0, \pi/2)$ are associated to the different signals of the eigenvalues. From the normalized eigenvectors, the relation $\mathbb{X} = \mathbb{B}\mathbb{R}\mathbb{B}^T$, can be obtained, with a diagonal matrix $\mathbb{R} = \text{Diag}[\lambda_1, -\lambda_1, \lambda_2, -\lambda_2]$ and the transformation matrix $\mathbb{B} = \mathbb{B}\mathbb{S}(t_1, t_2)\mathbb{B}\mathbb{B}\mathbb{S}$ described by the successive application of a pair of balanced beam splitters ($\mathbb{B}\mathbb{B}\mathbb{S}$), leading to the generation of two

mode squeezed states, followed by a mixing of each arm of these modes in beam splitters with specific transmission t_1, t_2 for the amplitudes of the fields, described by $\mathbb{BS}(t_1, t_2)$.

Direct calculation shows that

$$\begin{aligned}
 \chi_{12} &= -t_1 \lambda_1 t_2 - \sqrt{1-t_1^2} \lambda_2 \sqrt{1-t_2^2}; \\
 \chi_{13} &= t_1 \lambda_1 \sqrt{1-t_2^2} - \sqrt{1-t_1^2} \lambda_2 t_2; \\
 \chi_{24} &= \sqrt{1-t_1^2} \lambda_1 t_2 - t_1 \lambda_2 \sqrt{1-t_2^2}; \\
 \chi_{34} &= -\sqrt{1-t_1^2} \lambda_1 \sqrt{1-t_2^2} - t_1 \lambda_2 t_2,
 \end{aligned} \tag{4}$$

thus demonstrating that the decomposition presented in Figure 1 satisfies the modeling of the evolution of the operator under the Hamiltonian Equation 1. An interesting feature observed in the model involves the balanced photon generation involving pairs of modes (1,4) and (2,3). Since $[\hat{H}_I, \hat{n}_1 + \hat{n}_4] = [\hat{H}_I, \hat{n}_2 + \hat{n}_3]$, the number of photons generated in the upper part matches the number of photons generated in the lower part of the diagram, for any values of the coupling parameters χ_{ij} . On the other hand, imbalance in the photon generation involving pair of modes, as the one observed by the variances of the results in the main paper, can be modeled by the transmission coefficients t_1 and t_2 .

II. FOUR WAVE MIXING IN THE ATOMIC CLOUD

The distinct couplings involving the pump fields leads to pairwise production of photons in four distinct, yet coupled, modes, as depicted in Figure 1. This process involves the combination of different processes involving the composite level system of electronic and momentum degrees of freedom, as described in Figure 2(a). For instance, the interaction of the signal S_1 and a pump P_1 with the cloud generates a coherence grating between the states $|m, \vec{p}\rangle$ and $|m+1, \vec{p} + \hbar\vec{k}_{P_1} - \hbar\vec{k}_{S_1}\rangle$ (Fig 2(b)). A second interaction with the pump field P_1 brings the atom back to the state $|m, p\rangle$ generating the signal S_3 with wave vector $\vec{k}_{S_3} = 2\vec{k}_{P_1} - \vec{k}_{S_1}$, satisfying nearly phase matching condition, through forward FWM. Moreover, the same coherence grating involving fields P_1 and S_1 can also scatter light from the pump field P_2 , generating the signal S_2 , with wavevector $\vec{k}_{S_2} = -\vec{k}_{S_1}$ through the usual backward FWM process (Fig 2(c)). Finally, the present polarization configuration also generates the signal S_2 due to purely Recoil-Induced Resonance FWM associated with the scattering of the pump field P_1 into the atomic density grating created by the field P_2 and the signal field S_1 which has the same polarization (Fig 2d).

If the efficiency is sufficiently high, the generated beams S_2 and S_3 act as seeding beams to generate S_1 and S_4 , with wave vectors $\vec{k}_{S_1} = -\vec{k}_{S_2}$ and $\vec{k}_{S_4} = -\vec{k}_{S_3}$ and with the indicated polarization in Figure 1. As one can see from the symmetry, S_1 and S_4 couple parametrically with the pumping beams to generate S_2 and S_3 again, closing the loop. As one increases the pump power, the gain starts to build up, and the system oscillates as a mirrorless optical parametric oscillator (MOPO) [1, 2] with a threshold defined by the transition from a single pass regime to a feedback loop regime.

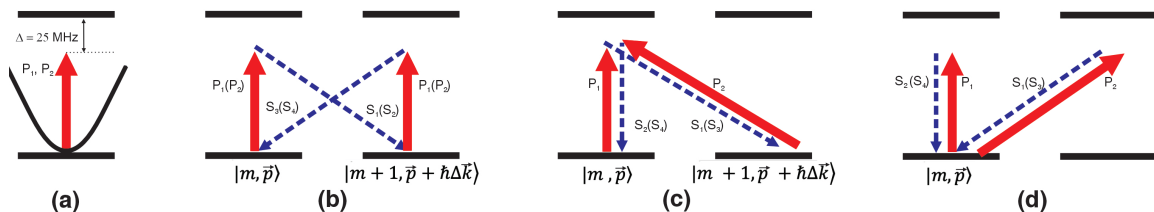


FIG. 2: Cesium hyperfine levels associated with the closed transition $6S_{1/2}, F=4 \rightarrow 6P_{3/2}, F'=5$. The parabola represents the atomic kinetic energy. (a) The composite system state is given by the direct product of the electronic Zeeman state $|m\rangle$ and momentum state $|\vec{p}\rangle$. (b), (c) and (d) Show generic interaction diagram associated with the different four-wave mixing processes.

III. EXPERIMENTAL SETUP

The magneto-optical trap (MOT), as previously described in [2], provided a cloud of roughly 10^6 Cs atoms at a temperature of the order of hundreds of μK .

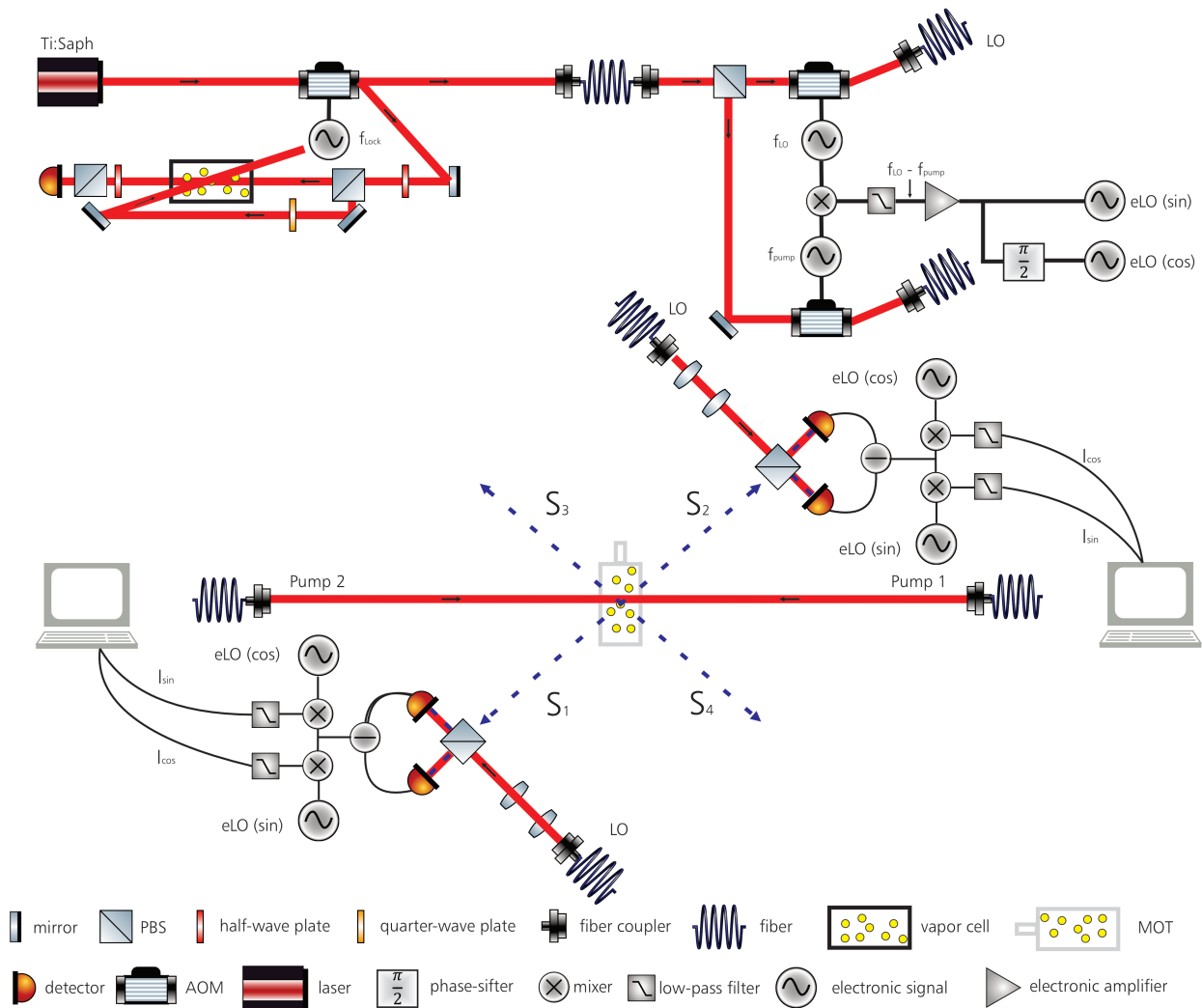


FIG. 3: Experimental setup.

The detailed setup, presented in Figure 3, involves the stabilization of a Ti:sapphire laser (Coherent 899). Part of the field is shifted up by an acousto-optic modulator driven by a frequency $f_{Lock} = 125.5$ MHz, and stabilized to the $F = 4 \rightarrow F' = 5$ transition using a polarization spectroscopy technique [6], thus providing a stable light source for measurement, red detuned from the cycling transition, with its noise reduced to the standard quantum level.

This laser beam is split in two parts. The first one, used for the pumping of the cold atoms cloud, has its frequency increased by an acousto-optic modulator coupled to a driver operating at $f_{pump} = 100.5$ MHz. This AOM has the double function of switching the beam during the cycle, controlling its power and frequency to optimize the gain of the parametric amplifier. Another part of the beam is shifted by a second acousto-optic modulator driven at $f_{pump} = 105.5$ MHz to be used as the optical local oscillator. The signal of both drivers, after proper mixing, low-pass filtering, electronic limitation and amplification, provides a pair of electronic local oscillators (eLO), where a phase shift ensures that both signals are in quadrature and with controlled amplitude for the detection process. As described in the next section, this is a fundamental part of the detection process, that will include an electronic reference at exact value of the detuning of the fields that are interfering in the optical detection. This coherence in the electronic part is fundamental for the measurement of the generated state by a combination of optical and electronic demodulations that are permanently turned on, thus allowing for a continuous sampling of the signal or, in

its absence, of the standard noise level of vacuum.

Spatial filtering and stabilization of the involved fields is ensured by the fiber coupling of pump and local oscillator beams into optical fibers, providing the balanced splitting of the pump fields sent over the atomic cloud, and the power control of the local oscillator in the balanced detection scheme. Pump beams have a large waist of 0.8 mm ($1/e^2$ radius), matching the size of the atomic cloud. Local oscillators have an input power of 2 mW, split between the input ports of a pair of balanced detectors (PDB465A, Thorlabs, quantum efficiency of 62% at 852 nm), measuring the fields S_1 and S_2 . Implementation of the detection for S_3 and S_4 , providing full characterization of the four fields, is under way.

A critical point in the setup is the matching of the correlated modes produced by the atomic cloud. As observed in [2], injection of a weak seed provides the generation of four beams in the outputs. Thus, careful alignment of the local oscillators, aiming at a maximized mode-matching with the input fields coming from the cloud, is provided by the injection of a seed along mode S_1 . The local oscillators' frequency is then shifted to a difference of hundreds of kHz from the pump frequency, and then are mode matched to the generated pulses by the optimization of the contrast of the beatnote of the fields observed in the subtraction signal of the balanced detection. This mode matching is challenged by the pulsed generation of the fields, with a duration of $\simeq 300\mu\text{s}$, and their spatial profile, depending on the overlap of the seed, the pump fields, and the cloud. Careful optimization of the gain and balance of the generated fields provides an optimal overlap of 0.9 with the Gaussian LO modes, with typical values in the range of 0.8. It is interesting to notice that, in the measurement, the seed is blocked and the parametric amplification of the vacuum modes provide a wide angle thermal output. Thus, simultaneous alignment of the matching of S_1 and S_2 will be critical for the correlation of the observed signals, but will not affect dramatically the variance observed on each signal. The goal here is having both homodyne detections observing the conjugated fields.

The final step involves the in-quadrature demodulation of the fast output of the balanced detectors. as we can see next, this in quadrature detection allows the simultaneous measurement of both quadratures of the field, at the cost of an extra unit of vacuum noise in the measurement.

IV. DETECTION THEORY

For the detailed treatment of the detection process, we recall that the photon-induced current in photodiodes can be associated to the expectation value of the intensity operator $\langle \hat{I}(\mathbf{r}, t) \rangle = \langle \hat{E}^-(\mathbf{r}, t) \hat{E}^+(\mathbf{r}, t) \rangle$, where field operator

$$\hat{E}^+(\mathbf{r}, t) = \sum_{\omega>0} \varepsilon_{\omega} \hat{a}_{\omega} e^{i(\mathbf{k}\cdot\mathbf{r}-\omega t)} \quad (5)$$

and its conjugate are the non-Hermitian operators related to the process of emission and absorption of photons in a mode of frequency ω , incident on the photodetector. While this current can give a limited access to the field information, restricted to the observable value of number operators \hat{n} , the combination of a local oscillator in homodyne and heterodyne detections converts the phase in amplitude fluctuations [4] which can be observed at the mean intensity measured by the photodiodes. The outputs of the beam splitter thus present a combination of the incoming fields: $\hat{E}^+(t) \propto \hat{E}_{LO}^+(t) \pm \hat{E}_S^+(t)$, and the subtraction of the photocurrents is proportional to the interference term

$$I(t) \propto \langle \hat{E}_{LO}^+(t) \hat{E}_S^-(t) + \hat{E}_{LO}^-(t) \hat{E}_S^+(t) \rangle. \quad (6)$$

If we use a coherent state $|\alpha_{\omega_{LO}}\rangle$ as the input for the LO mode, with an amplitude given by $\alpha = |\alpha|e^{i\varphi}$, while describing the measured state by $|\psi\rangle$, the global state is written as $|\Psi\rangle = |\alpha_{\omega_{LO}}\rangle \otimes |\psi\rangle$. Substituting in Equation 6, the resulting photocurrent is

$$I(t) \propto |\alpha| \left\langle \psi \left| \left(e^{-i\varphi} \int d\omega' e^{-i(\omega'-\omega_{LO})t} \hat{a}_{\omega'} + e^{i\varphi} \int d\omega' e^{i(\omega'-\omega_{LO})t} \hat{a}_{\omega'}^{\dagger} \right) \right| \psi \right\rangle. \quad (7)$$

Upon photodetection and electronic filtering, the integrals will be involving only modes whose frequency ω' is close to the local oscillator frequency ω_{LO} . Many experimental implementations associate bosonic operators to the combinations of the contributions of each mode near the local oscillator mode [5], as

$$\hat{a}(t) = \int' d\omega e^{-i(\omega-\omega_{LO})t} \hat{a}_{\omega} \quad , \quad \hat{a}^{\dagger}(t) = \int' d\omega e^{i(\omega-\omega_{LO})t} \hat{a}_{\omega}^{\dagger},$$

integrated over the detector bandwidth (signaled by the prime), yielding

$$I(t) \propto |\alpha| \left\langle \hat{X}_{\varphi}(t) \right\rangle, \quad \text{where} \quad \hat{X}_{\varphi}(t) = e^{-i\varphi} \hat{a}(t) + e^{i\varphi} \hat{a}^{\dagger}(t) \quad (8)$$

is the quadrature operator of the field.

Notice that the current in Equation 8 involves a wide combination of frequency terms resulting from the beatnote between the carrier and the sideband modes, that we label by $\Omega = \omega - \omega_{LO}$. While the usual homodyne detection returns a combination of the modes within the bandwidth of the detectors, one can narrow the measurement to a specific mode using demodulation techniques such as the one performed by a spectrum analyzer or a demodulation chain. The usual procedure to filter out the information at a given frequency is to amplify and electronically mix the measured photocurrent with an electronic local oscillator (eLO) with frequency Ω_0 and phase θ , whose current is

$$I_0(t) \propto e^{i(\Omega_0 t + \theta)} + e^{-i(\Omega_0 t + \theta)}, \quad (9)$$

yielding the following result after the mixer

$$\begin{aligned} I_{\text{mix}}(t) &\propto I(t)I_0(t) \\ &= \left\langle e^{-i\varphi} e^{i\theta} \int_{-\infty}^{\infty} d\omega' e^{-i(\omega' - \omega_{LO} - \Omega_0)t} \hat{a}_{\omega'} + e^{i\varphi} e^{-i\theta} \int_{-\infty}^{\infty} d\omega' e^{i(\omega' - \omega_{LO} - \Omega_0)t} \hat{a}_{\omega'}^\dagger \right. \\ &\quad \left. + e^{-i\varphi} e^{-i\theta} \int_{-\infty}^{\infty} d\omega' e^{-i(\omega' - \omega_{LO} + \Omega_0)t} \hat{a}_{\omega'} + e^{i\varphi} e^{i\theta} \int_{-\infty}^{\infty} d\omega' e^{i(\omega' - \omega_{LO} + \Omega_0)t} \hat{a}_{\omega'}^\dagger \right\rangle. \end{aligned} \quad (10)$$

This resulting current is finally averaged by a low-pass filter, that will select a specific combination involving pairs of modes. Thus, from the averaging, we obtain

$$\begin{aligned} I_{\text{out}} &= \int_{-\infty}^{\infty} I_{\text{mix}} dt \\ &\propto \left\langle e^{-i(\varphi - \theta)} \hat{a}_{\omega_{LO} + \Omega} + e^{i(\varphi - \theta)} \hat{a}_{\omega_{LO} + \Omega}^\dagger + e^{-i(\varphi + \theta)} \hat{a}_{\omega_{LO} - \Omega} + e^{i(\varphi + \theta)} \hat{a}_{\omega_{LO} - \Omega}^\dagger \right\rangle, \end{aligned} \quad (11)$$

where we used

$$\delta(\omega - \omega') = \frac{1}{2\pi} \int_{-\infty}^{+\infty} dt e^{i(\omega - \omega')t}. \quad (12)$$

The resulting value of I_{out} can be registered by an analog-to-digital converter. Higher order momenta can be computed from the numerical statistical analysis of the acquired data.

As we can see, the typical combination of optical and electronic local oscillators will return a combined measurement of observables of a pair of modes, symmetric to the optical local oscillator frequency ω_{LO} , involving the beatnote of the upper and lower sidebands, shifted from the LO frequency by $\pm\Omega$. In the usual homodyne detection, the field under investigation, described by the operator $\hat{a}(t)$, has a central frequency ω_S and is studied over its sidebands by sweeping the frequency of the electronic oscillator. Equation 11 can be rewritten with the help of operators for the quadratures, $\hat{p}_\Omega = \hat{a}_\Omega + \hat{a}_\Omega^\dagger$ and $\hat{q}_\Omega = -i(\hat{a}_\Omega - \hat{a}_\Omega^\dagger)$, as

$$I_{\text{out}} \propto \left\langle \cos(\varphi - \theta) \hat{p}_{\omega_{LO} + \Omega} + \sin(\varphi - \theta) \hat{q}_{\omega_{LO} + \Omega} + \cos(\varphi + \theta) \hat{p}_{\omega_{LO} - \Omega} + \sin(\varphi + \theta) \hat{q}_{\omega_{LO} - \Omega} \right\rangle \quad (13)$$

thus involving a balanced combination of upper and lower sidebands, as depicted in (Figure 4a).

However, we are interested in a narrow-band signal such as the one seen in RIR, whose bandwidth is in the $2\pi \times 10$ kHz range around the pump mode frequency [2]. Direct homodyning in this case will bring all the problems involving noise sources at lower frequencies that affect the direct electronic measurement of homodyne techniques, and lead to the generalized use of spectrum analyzers for measurement of the momenta of quadrature operators. In the present case, we combine the electronic oscillator at an analysis frequency of $\Omega = 5$ MHz, while setting the optical local oscillator frequency shifted by this same amount relative to the pump fields. Therefore the mode of interest will be sitting in one of the sidebands of the local oscillator, resolved by the demodulation chain associated to the optical homodyne detection, with the cost of adding the measurement of another mode. Fortunately, this empty mode presets only vacuum fluctuations, that can be discarded on the analysis of the results (Figure 4b)

The resulting measurement for this heterodyne detection presents a combination involving the quadratures of the mode (i) of interest and one mode of vacuum (0):

$$I_{\text{out}} \propto \langle \hat{I}_{\text{out}}(\varphi, \theta) \rangle = \frac{1}{\sqrt{2}} \left\langle \cos(\varphi - \theta) \hat{p}_i + \sin(\varphi - \theta) \hat{q}_i + \cos(\varphi + \theta) \hat{p}_0 + \sin(\varphi + \theta) \hat{q}_0 \right\rangle. \quad (14)$$

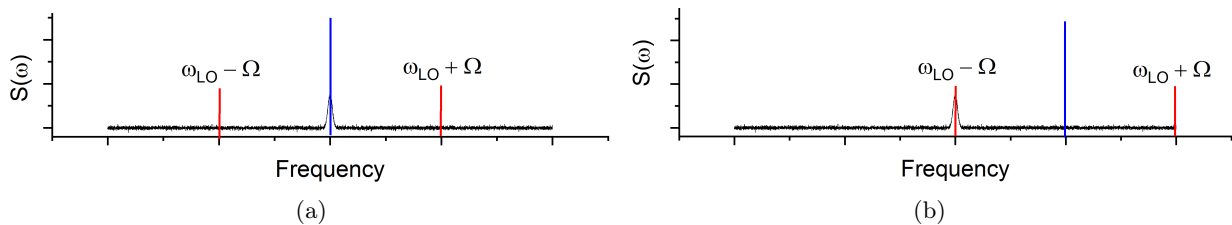


FIG. 4: Sidebands and local oscillator at the homodyne and heterodyne detections. The signal under analysis corresponds to the Lorentzian peak, centered at the pump frequency. Left: with the local oscillator field (marked in blue), at the pump frequency, the measured modes using the electronic demodulation (marked in red) will be sitting in a range of frequencies involving only vacuum fluctuations. Right: By shifting the optical local oscillator by the analysis frequency Ω , the mode of interest will be detected, along with another mode associated to a vacuum state.

The choice of the observed quadrature could be performed by changing the optical phase φ , but the presence of the electronic phase allows for the simultaneous observation of both quadratures of field i by splitting the photocurrent and combining in-quadrature demodulation. We can define an arbitrary choice of $\theta = 0$, giving

$$\hat{I}_{\cos} = \hat{I}_{out}(\varphi, 0) = \frac{\cos(\varphi)\hat{p}_i + \sin(\varphi)\hat{q}_i + \cos(\varphi)\hat{p}_0 + \sin(\varphi)\hat{q}_0}{\sqrt{2}}, \quad (15)$$

and its counterpart for an in-quadrature demodulation $\theta = \pi/2$

$$\hat{I}_{\sin} = \hat{I}_{out}(\varphi, \pi/2) = \frac{\sin(\varphi)\hat{p}_i - \cos(\varphi)\hat{q}_i - \sin(\varphi)\hat{p}_0 + \cos(\varphi)\hat{q}_0}{\sqrt{2}}. \quad (16)$$

Simultaneous access to both quadratures of field i is thus guaranteed. For instance, when $\varphi = 0$, we have

$$\hat{I}_{\cos} = \frac{\hat{p} + \hat{p}_0}{\sqrt{2}} = \hat{p}' \quad \text{and} \quad \hat{I}_{\sin} = \frac{\hat{q} - \hat{q}_0}{\sqrt{2}} = \hat{q}'. \quad (17)$$

Optical shifting of the local oscillator will sweep the Fresnel plane, giving always a pair of conjugate operators of the field. The simultaneous access to these quadratures, then, comes with the addition of one unit of vacuum noise. This drawback in the quantum characterization of the mode is not dramatically restrictive, though, since this additional noise can always be suppressed in the posterior evaluation of the covariance matrix of the mode of interest.

Simultaneous registration of in-quadratures measurements issued from homodyne detection of both detectors are used to reconstruct the covariance matrix, with the ultimate goal of evaluating the entanglement criteria in continuous variables, such as the test of positivity under partial transposition [8]. As we have shown, the I_{\cos} and I_{\sin} are associated to the \hat{p} and \hat{q} quadratures. It would be straightforward to calculate the terms of

$$\mathbb{V} = \frac{1}{2} \left\langle \hat{\xi}\hat{\xi}^T + \left(\hat{\xi}\hat{\xi}^T \right)^T \right\rangle, \quad (18)$$

where $\hat{\xi} = (\hat{p}_1, \hat{q}_1, \hat{p}_2, \hat{q}_2)^T$, if we didn't have a vacuum component in our detection.

The added vacuum term in Equation 17 can be further suppressed in the final characterization of the state, if we notice that the transformation is equivalent to a beam splitter transformation, such as $\hat{a}_{out} = \sqrt{\eta}\hat{a}_{in} + \sqrt{1-\eta}\hat{b}_{in}$, with $\eta = 0.5$, equivalent to the modeling of an inefficient detector with a particular quantum efficiency. The final matrix \mathbb{V} of the desired covariances relate to the measured matrix \mathbb{V}' as

$$\mathbb{V}' = \eta(\mathbb{V} - \mathbb{I}) + \mathbb{I} \rightarrow \mathbb{V} = 2 \cdot \mathbb{V}' - \mathbb{I}. \quad (19)$$

As we can see, detection benefits from the fact that the measured observables, that form an EPR-type set of observables, are relating our field of interest to a completely uncorrelated vacuum frame.

V. STATISTICS OF THE DATA

Differently from the majority of the CV systems, which have continuous generation of the modes, the amplification by a (MOT) involves a pulsed system which only allows measurements in the meantime between the interruption of

the trapping fields, while the atoms were not lost due to ballistic expansion of the cloud or due to optical pumping by the pump fields. This gives a window with up to 1.6 ms, after which a new cloud is formed by trapping and cooling back the atoms in a new cycle of 23 ms.

Moreover, the narrow bandwidth of the (RIR) imposes a limit on the acquisition rate. Keeping the bandwidth of the low pass filter of the detection compatible with the parametric amplification bandwidth of ≈ 20 kHz, defining thus the spectral mode under evaluation, an acquisition rate greater than twice this value would be redundant. Thus the acquisition time of $25 \mu\text{s}$ ($= 1/40$ kHz) [2], leave us with 64 points per cycle. This is statistically insufficient for a faithful reconstruction of the covariance matrix, in order to observe entanglement. Therefore, it is necessary to evaluate the average of measurements over several MOT cycles.

However, averaging the covariance matrices terms for distinct runs suffers from distinct sources of phase diffusion. The first one involves the coherence of the optical and electronic oscillators. The whole evolution of the system develops on the time frame of the pump field, that is phase related to the optical local oscillator by their common source. Any disturbance between them would come from the electronic driver. Coherence of the electronic local oscillator for heterodyne measurement is assured since it is directly derived from the beatnote of both beams. Interferometric arrangement over the optical table, in the optical homodyning, can be an issue, but the verified stability involves drifts of the order of tens of seconds, thus hundreds of runs of the MOT, and in principle is not the main issue.

On the other hand, the distinct experimental conditions from one MOT to another are an important point to be considered. Every trapping and cooling cycle will involve some loss and some inclusion of new atoms in the cloud, whose center of mass can displace slightly from one run to another, depending on small fluctuations of the trapping lasers. While these fluctuations are negligible from the point of view of a mm sized MOT, they may imply in a dramatic change in the position of the amplifier in the heart of the generation of the fields, in the order of the wavelength. Thus their phase may suffer a strong drift from one run to another. Therefore, we have to take into account the role of these random phase shifts in the analysis of entanglement.

Consider the covariance matrix in the special form [7, 8]

$$\mathbb{V}_0 = \begin{bmatrix} a_1 & 0 & c_1 & 0 \\ 0 & a_1 & 0 & c_2 \\ c_1 & 0 & a_2 & 0 \\ 0 & c_2 & 0 & a_2 \end{bmatrix}. \quad (20)$$

Any covariance matrix, such as the one given by Equation 18, can be brought to this special form by a suitable sequence of local canonical transformations, involving noise compression and phase rotations. Starting from a general matrix of the form

$$\mathbb{V} = \begin{bmatrix} \mathbb{A}_1 & \mathbb{C} \\ \mathbb{C}^T & \mathbb{A}_2 \end{bmatrix}, \quad (21)$$

the properties of entanglement and purity can be directly evaluated from symplectic invariants, particularly the determinants of matrices \mathbb{A}_1 , \mathbb{A}_2 , \mathbb{C} , and \mathbb{V} . Thus, instead of evaluating directly the elements of matrix 18 under distinct runs, due to statistical limitations from the fluctuating experimental conditions, we will evaluate the average of the invariants, applying some considerations over the phase rotations.

For the quadratures of a given mode, a shift in the phase would correspond to a rotation in the Fresnel plane of the form

$$\begin{bmatrix} \hat{p}' \\ \hat{q}' \end{bmatrix} = \begin{bmatrix} \cos \theta & -\sin \theta \\ \sin \theta & \cos \theta \end{bmatrix} \begin{bmatrix} \hat{p} \\ \hat{q} \end{bmatrix} = \mathbb{R}_\theta \begin{bmatrix} \hat{p} \\ \hat{q} \end{bmatrix}. \quad (22)$$

It is evident that the submatrices \mathbb{A}_1 and \mathbb{A}_2 are invariants under rotation ($\mathbb{R}_\theta \mathbb{A}_i \mathbb{R}_\theta^\dagger = \mathbb{A}_i$).

Considering now that our system is expected to produce quadrature correlations such as $c_1 = -c_2 = c$, phase rotations on each mode will result in

$$\mathbb{C} = \mathbb{R}_{\theta_1} \mathbb{C}' \mathbb{R}_{\theta_2}^\dagger = c \begin{bmatrix} \cos \phi & \sin \phi \\ \sin \phi & -\cos \phi \end{bmatrix}, \quad (23)$$

where $\phi = \theta_1 + \theta_2$. Thus, the measured covariance matrix will have the form

$$\mathbb{V}' = \begin{bmatrix} a & 0 & c \cos \phi & c \sin \phi \\ 0 & a & c \sin \phi & -c \cos \phi \\ c \cos \phi & c \sin \phi & b & 0 \\ c \sin \phi & -c \cos \phi & 0 & b \end{bmatrix}.$$

Each run of the MOT will provide distinct outputs for the elements of the correlation matrix \mathbb{C} , varying randomly with the phase changes of the output fields, then averaging to zero over many repetitions. Nevertheless, the determinant on each run can be evaluated, and their value should converge to

$$\text{Det}[\mathbb{C}] = - \langle c^2 \cos^2 \varphi + c^2 \sin^2 \varphi \rangle = -c^2. \quad (24)$$

This reasoning can be applied since the contribution of statistical fluctuations of the cross correlation involving distinct detections, with other origin than the phase diffusion, will average to zero.

This reasoning cannot be applied to the covariance evaluated for each mode. Consider that on each run a matrix of the form

$$\mathbb{A} = \begin{bmatrix} \Delta^2 p & c_{pq} \\ c_{pq} & \Delta^2 q \end{bmatrix} \quad (25)$$

is reconstructed. Since $\text{Det}[\mathbb{A}] = \Delta^2 p \cdot \Delta^2 q - c_{pq}^2$, contribution of random fluctuations from insufficient sampling in $\Delta^2 p$ and $\Delta^2 q$ will vanish upon the average of many runs. On the other hand, fluctuations in the cross correlations of the simultaneous measurement of quadratures \hat{p} and \hat{q} , used to determine $c_{pq} = \langle \hat{p}\hat{q} \rangle$, will provide an underestimation of $\text{Det}[\mathbb{A}]$ from the evaluation of the determinant on each acquisition. In this case, it is better to evaluate separately the statistics of $\Delta^2 p$, $\Delta^2 q$ and c_{pq} , and compare the evolution of each distribution, that evolves to $\Delta^2 p = \Delta^2 q = a$ and $c_{pq} = 0$, and use $\text{Det}[\mathbb{A}] = a^2$.

Thus, even though we cannot obtain the full covariance matrix after averaging over many MOT cycles, we can still use the determinants $\text{Det}[\mathbb{A}_1] = a_1^2$, $\text{Det}[\mathbb{A}_2] = a_2^2$, $\text{Det}[\mathbb{C}] = -c^2$ to evaluate $\text{Det}[\mathbb{V}]$ and then the test of physicality and entanglement presented in the PPT criterium [8].

-
- [1] A. Schilke and C. Zimmermann and P. W. Courteille and W. Guerin, *Optical parametric oscillation with distributed feedback in cold atoms*, Nature Photonics **6**, 101-104 (2011).
 - [2] J. P. Lopez, A. M. G. de Melo, D. Felinto, and J. W. R. Tabosa, *Observation of giant gain and coupled parametric oscillations between four optical channels in cascaded four-wave mixing*, Phys. Rev. A **100**, 023839 (2019).
 - [3] S. L. Braunstein, *Squeezing as an irreducible resource*, Phys. Rev. A **71**, 055801 (2005).
 - [4] H. P. Yuen and V. W. Chan, *Noise in homodyne and heterodyne detection*, Opt. Lett. **8**, 177-179 (1983).
 - [5] F. A. S. Barbosa, A. S. Coelho, K. N. Cassemiro, P. Nussenzveig, C. Fabre, A. S. Villar, and M. Martinelli, *Quantum state reconstruction of spectral field modes: homodyne and resonator detection schemes*, Phys. Rev. A **88**, 052113 (2013).
 - [6] C. Wieman, T. W. Hänsch, *Physical Review Letters, Doppler-free laser polarization spectroscopy*, Physical Review Letters **36**, 1170, (1976).
 - [7] Lu-Ming Duan, G. Giedke, J. I. Cirac, and P. Zoller, *Inseparability Criterion for Continuous Variable Systems*, Phys. Rev. Lett. **84**, 2722 (2000).
 - [8] R. Simon, *Peres-Horodecki separability criterion for continuous variable systems*, Phys. Rev. Lett. **84**, 2726 (2000).